

**Considering impacts associated to simultaneous perils: integrating  
tsunamigenic and seismic risk within the R-CAPRA fully probabilistic loss  
assessment framework**

**Mario Ordaz,**

**Instituto de Ingeniería, UNAM, Mexico City, Mexico**

**ERN, Mexico City, Mexico**

**Mario A. Salgado-Gálvez, Benjamín Huerta, Juan C. Rodríguez, Carlos E. Avelar,**

**ERN, Mexico City, Mexico**

## Introduction

Several countries around the globe, as shown in Figure 1, can face catastrophe losses inflicted by perils of different types. Some of these perils have complex interactions between them so that, in practical terms, their effects act in a simultaneous manner over the exposed population and built infrastructure. Despite the recent development of openly available risk assessments with multi-hazard features (e.g., GAR15), the interaction between the considered perils has been overlooked.

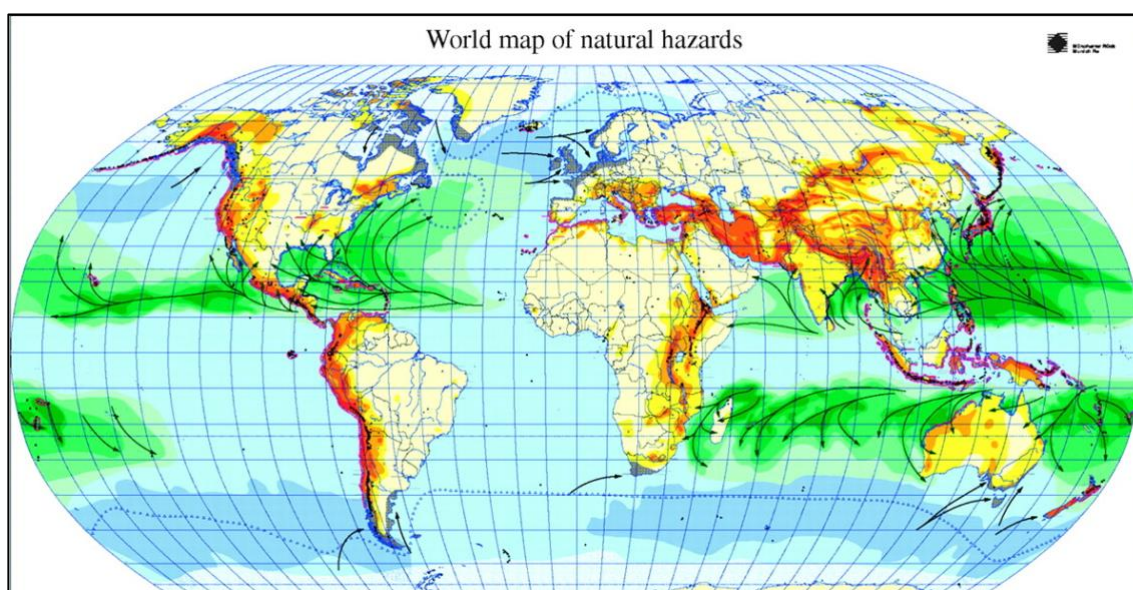


**Figure 1. World map of natural hazards. Source: MunichRe**

Countries located near subduction zones, such as for instance Mexico, Chile, Peru, Japan and Indonesia, can be affected by both earthquakes and tsunamis. In general, for the generation of a tsunami, a prior event with the capability of displacing large volumes of water needs to occur. Although these detonating events are of different types, most of them are earthquakes. When this kind of earthquakes occur at close distances from the coastal areas, damages and losses on the exposure are caused not only because of the tsunami waves but also from the ground motion itself.

The development of multi-hazard risk assessment frameworks has gained momentum in the recent past, aiming to provide a complete risk panorama at locations and portfolios exposed to the occurrence of different perils. Nevertheless, for a proper risk quantification, on which under or overestimations should not occur, a rigorous consideration of the losses caused by simultaneous events needs to be made, being consistent at the same time with the usual assumptions made by these models.

A simple but novel approach to address these issues was proposed by Ordaz (2015) and is currently implemented in R-CAPRA (ERN, 2018), where, still considering the losses associated to each of the individual hazards as random variables, the probability distribution of the combined loss is obtained. The combination rule can be considered as peril-agnostic, meaning that its application can be expanded to the case of earthquakes and tsunamis but also to hurricanes, where strong winds, floods and surge are hazard intensities that also occur at the same time.

R-CAPRA is the latest version of the CAPRA risk assessment tool, a well-known, widely used and open-source and flexible software architecture program that has been adopted by the United Nations Office for Disaster Risk Reduction (UNISDR) in the development and application of its Global Risk Model (GRM) since 2012 (UNISDR, 2013; 2015a; 2017). R-CAPRA has the flexibility to incorporate into the analyses perils of different types (e.g., earthquakes, tsunamis, hurricanes, floods, hail, drought, wildfires) and its methodology is completely scalable, meaning that very detailed and high resolution, or less detailed and coarse-grain analyses can be performed. This tool incorporates state-of-the-art methodologies that allow the development of peril-agnostic and fully probabilistic risk assessments on different types of exposures and at different scales, ranging from the built environment to networks (e.g., roads and water sanitation systems) together with the agricultural sector (i.e., to assess losses caused by droughts).



The Sendai Framework for Disaster Risk Reduction –SFDRR– (UNISDR, 2015b) promotes the quantification of risk due to multiple perils with different origins (e.g., natural, technological, anthropogenic) aiming to notably decrease their impacts, by 2030, in terms of economic and human losses. For this to occur, a proper risk quantification process needs to be made to comply with some of the goals included in the Priority 1, and in multi-hazard environments, the proper consideration and aggregation of losses for simultaneous perils is required. Although the GRM has clearly marked a milestone in the prospective and probabilistic modelling at global level, it has the disadvantage that not all the relevant risk metrics can provide a robust multi-hazard overview. Even that the GRM has data about different hazards that are interconnected among them, (e.g., earthquakes and tsunamis;

cyclonic wind and storm surge), the assessment of the future losses has been performed in a separate manner. This yields in that only average annual multi-hazard losses can be approximately estimated by adding individual AALs for each of the perils, failing to provide a complete risk panorama achieved only when other metrics such as the LEC and PML are available.

This paper presents the application of the methodology at two different locations in Latin America: Acapulco (Mexico) and Callao (Peru) where results are obtained in terms of commonly used risk metrics, besides hazard and risk maps, exemplifying how a similar methodology that the one followed by the GRM can be applied, at a more detailed scale (for the hazard and exposure components), and also providing a robust multi-hazard risk overview of the two domains under study.

The paper is subdivided into sections on which the methodological summary is included, followed by the application of the methodology at two locations in Mexico and Peru. Finally, the discussion of the results is complemented with some ideas around the integration of the methodology within the UNISDR's GRM, aiming to make out the most from the currently available datasets and pointing out specific actions needed for the future integration of these perils by considering in a robust manner their interactions.

## **Fully probabilistic loss assessment methodology**

### **Seismic hazard analysis**

The classic procedure for performing a probabilistic seismic hazard analysis (PSHA) has its roots on the ideas of Esteva (1967) and Cornell (1968) where in summary, the area under analysis is divided into zones on which seismicity can be assumed to have the similar characteristics in terms of maximum magnitudes, magnitude recurrence frequencies and attenuation patterns. Using data from historical earthquakes, different parameters are estimated describing the future occurrence of earthquakes within any place inside the limits of these areas. Finally, by means of attenuation relationships, the ground motion intensities (physical measures such as spectral acceleration) are estimated as a function of usually, at least, magnitude and distance.

On this process, different uncertainties are accounted for, as for instance, the location, magnitude, attenuation pattern and frequencies of occurrence of future earthquakes, reason why a probabilistic approach is needed. These uncertainties not only need to be identified but when possible quantified and propagated throughout the analysis.

Seismic hazard is usually expressed in terms of intensity exceedance rates,  $\lambda(a)$ , and is calculated with the following expression:

$$\nu(a) = \sum_{n=1}^N \int_{M_0}^{M_U} -\frac{\partial \lambda}{\partial M} \Pr(A > a | M, R_i) dM \quad (\text{Eq. 1})$$

where  $N$  is the total number of seismic sources within the integration distance,  $\Pr(A > a | M, R_i)$  is the probability that the intensity exceeds a certain value given the magnitude of the earthquake  $M$ , and the distance between the  $i^{\text{th}}$  source and the site of analysis,  $R_i$  and  $\lambda_i(M)$  represent the earthquake magnitude exceedance rates. The integration is performed between  $M_0$  to  $M_U$  (threshold and maximum magnitudes, respectively) which indicates that, for each source, the contribution of all possible magnitudes is considered.

Assuming that given a magnitude and a distance, the intensity follows a lognormal distribution, the probability  $\Pr(A > a | M, R_i)$  is calculated as follows:

$$\Pr(A > a | M, R_i) = \Phi \left( \frac{1}{\sigma_{Lna}} \ln \frac{\text{MED}(A | M, R_i)}{a} \right) \quad (\text{Eq. 2})$$

where  $\Phi(\cdot)$  is the normal standard distribution,  $\text{MED}(A | M, R_i)$  is the median of the intensity, given by the associated attenuation model for known magnitude and distance, and  $\sigma_{Lna}$  denotes the standard deviation of the natural logarithm of the intensity.

Intensity exceedance rates are calculated for different values obtaining what are known as hazard curves. From them, commonly used representations to communicate the hazard levels at the domain under study such as uniform hazard spectra and/or hazard maps can be obtained for any return period can be obtained.

As mentioned before, some types of earthquakes have the capability of triggering tsunamis after displacing large volumes of water. These events usually occur at subduction zones and have large magnitudes. It is for these seismic sources that the integration with the tsunamigenic hazard is needed. For each event that exceeds a certain magnitude threshold, two different processes are required: 1) estimation of ground motion intensities at the locations of interest (with the above-explained procedure) and, 2) generation of tsunamis requiring modelling their propagation and water run-up as explained with more details next.

## Tsunami hazard analysis

Using the PSHA data (i.e., each of the events occurring at the subduction zones with a magnitude higher than a specified threshold), the surface displacement of each tsunami-generating event is defined. Given the

occurrence of an earthquake with magnitude,  $M$ , and with a focus located at a seismic source capable of generating tsunamis, the rupture area is estimated. The corresponding seismic moment,  $M_0$ , is computed with the Hanks and Kanamori (1979) given by,  $\log_{10}M_0=1.5 \cdot M+16.05$ . From the relation,  $M_0=m \cdot A \cdot U$ , the average slip,  $U$ , on the fault, is obtained, assuming  $\mu=5 \times 10^4$  MPa (Singh et al. 2012). Finally, assuming a dip of the fault,  $\theta=15^\circ$ , for all tsunamigenic events, the vertical component of the slip is computed as  $U_z=U \cdot \sin(\theta)$ . With this, the calculation of the tsunami propagation and its intensity at the sites of interest is made. Several methods are available for tsunami modelling, either using empirical relations based on historical data (Okal and Synolakis, 2004) or by means of numerical simulations (LeVeque, 2002; LeVeque and George, 2007). The latter approach is preferred and used in the two case studies presented next to estimate the tsunami intensities, based on the GeoClaw tsunami model. GeoClaw is a well-known software for tsunami modelling and its source code is freely available<sup>1</sup>.

The GeoClaw numerical model has undergone extensive validation and verification tests for tsunami modelling using both synthetic test analysis and comparison with data from real events. These tests are based on comparing surface elevation or inundation (LeVeque and George, 2007; Berger et al., 2011; Gonzalez et al., 2011; LeVeque et al., 2011) besides quantitative comparisons of observed time series data (e.g. Arcos and LeVeque, 2013). The GeoClaw software implements high-resolution finite volume methods to solve the nonlinear shallow water equations, a depth-averaged system of partial differential equations in which the fluid depth  $h(x, y, t)$  and two horizontal depth-averaged velocities  $u(x, y, t)$  and  $v(x, y, t)$  are introduced as:

$$\begin{aligned} h_t + (hu)_x + (hv)_y &= 0 \\ (hu)_t + \left( hu^2 + \frac{1}{2}gh^2 \right)_x + (huv)_y &= -ghB_x - Dhu \\ (hv)_t + \left( hv^2 + \frac{1}{2}gh^2 \right)_y + (huv)_x &= -ghB_y - Dhv \end{aligned} \quad (\text{Eq. 3})$$

Subscripts denote partial derivatives. The momentum source terms on the right hand side include the bathymetry  $B(x, y, t)$  and  $D(h, u, v)$ , the drag coefficient.

Data required by the GeoClaw numerical model are the topography and bathymetry of the area under study. Several open data sources for bathymetry are available, such as the one developed by NOAA with a 500x500m resolution

---

<sup>1</sup> <http://depts.washington.edu/clawpack/>

level. For each tsunami event simulated with the GeoClaw model, the wave heights are computed at several reference points along the coastline. Once the wave height is computed for each reference point, the model provides the flood height at the sites where the exposed assets are located. The flood height is estimated as the difference between the wave height at the closest reference point and the elevation of the terrain, obtained from detailed topography.

## Event-based representation

Natural hazards can be represented in different manners, depending on the final use of the results. On one hand, hazard maps are useful for communication purposes although they are not sufficient for comprehensive (and fully probabilistic) risk assessments. On the other hand, stochastic event-sets, which are collections of feasible ways in which hazard may manifest and account for events that have not necessarily yet occurred. The latter representation, as summarized in Figure 2, uses a probabilistic representation by including (at least) the first two probability moments (expected value and standard deviation) and an occurrence frequency.

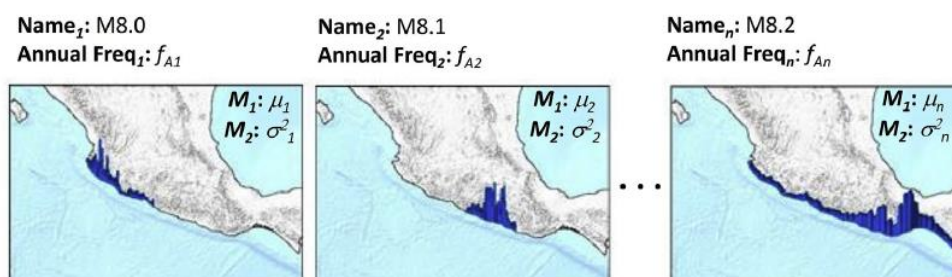


**Figure 2. Schematic representation of a stochastic event set (Source: Jaimes et al., 2016)**

The use of the second representation, which can also be considered as peril-agnostic (and therefore expanded to other hazards), is needed for the fully probabilistic estimation of losses, facilitating at the same time the consideration of simultaneous perils at the domain under study. In summary, for the integration of earthquake and tsunami hazard within the same risk assessment, two different stochastic event-sets are needed, one for each peril, where for each earthquake with the capability of triggering a tsunami, the corresponding tsunami hazard intensities are associated.

## Exposure databases

The development of exposure databases still constitutes a big challenge when dealing with probabilistic catastrophe losses. It is a mandatory stage where both, the identification and the characterization of the exposed assets that can be affected by the hazard intensities of the perils of interest is made. The identification phase includes the selection of assets that belong to a particular sector (i.e., housing, education, ports, railroads) and also their geolocation. The characterization phase includes the assignation of all relevant parameters that describe their performance under the solicitation of the hazard intensities (e.g., structural characteristics), together with an economic appraisal and in some cases, the definition of human occupancy values. For assigning each of these attributes there is no standardized procedure and for instance, when determining what is the economic value of an asset, in terms of its replacement cost, different indicators with roots in cadastral data and demographic and macroeconomic indexes are combined.

Exposure databases can be developed at different resolution levels, ranging from very detailed ones (i.e., asset by asset) to coarse-grained ones (e.g., GAR15). What resolution level to use depends not only in the data availability but also in the scope and expected outcomes of the risk assessment, together with limitations associated to computational capabilities and time, economic and human resources.

R-CAPRA allows the use of exposure databases with any resolution level and a common format for providing the identification and characterization data of each exposed asset. In summary, these data are:

- Unique identified
- Exposed value (replacement cost)
- Human occupancy (either scenario based or averaged)
- Identifier of the building class for each of the perils of interest

For the latter, there can be as many attributes as perils considered where, of course, for each of the perils different building classes can be identified. This attribute allows a posterior linkage between the exposure and the vulnerability data. All this information is stored in the database linked to a shapefile.

## Vulnerability representation

There are several ways on which damages (and losses) can be related to hazard intensities. These range from subjective damage index categories to more objective fragility curves and vulnerability functions. The latter

are preferred within fully probabilistic risk assessment frameworks, as the one used herein, since they have not only a continuous but probabilistic representation of the losses. Losses can have different dimensions, such as physical, human and environmental, among others. Within probabilistic risk assessment frameworks, usually the first two are considered although, in this paper, the focus will be made only on the first.

These functions can be obtained from different manners, such as empirically based (after surveying an affected area where the hazard intensities are known) but also through analytical and experimental models. It is common practice to combine these approaches for the derivation of the vulnerability models that are used in the risk assessments.

These functions are useful in the estimation of direct losses (those associated only to the structure and its contents) and are always capped at 100%, meaning that the maximum value of the loss cannot exceed the total exposed value. For each of the building classes identified in the exposure database (which can vary from hazard to hazard), for each of the perils, a unique vulnerability function is assigned.

The probabilistic representation of a vulnerability function is achieved by providing to the model the expected value of the loss, associated to different hazard intensity levels and a dispersion measure (usually made in terms of the standard deviation) of it. Figure 3 shows, schematically, the components of a probabilistic vulnerability function. A characteristic of these functions, regardless the hazard, is that dispersion values are minimum at very low and very high hazard intensity levels whereas the peak value of that parameter is usually associated to a loss value of 50%. Figure 4 shows an example of two vulnerability curves for tsunami: one and three story.

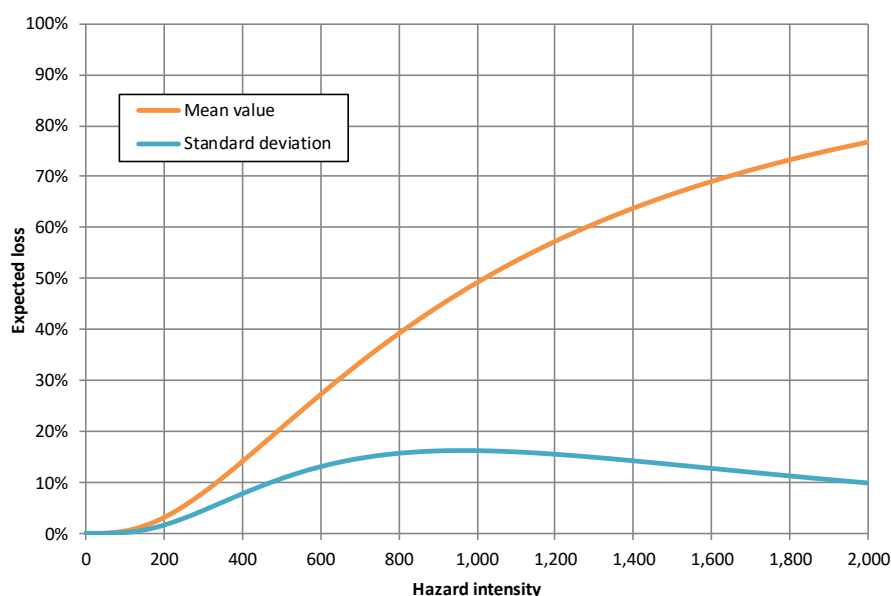


**Figure 3. Schematic representation of a physical vulnerability function**

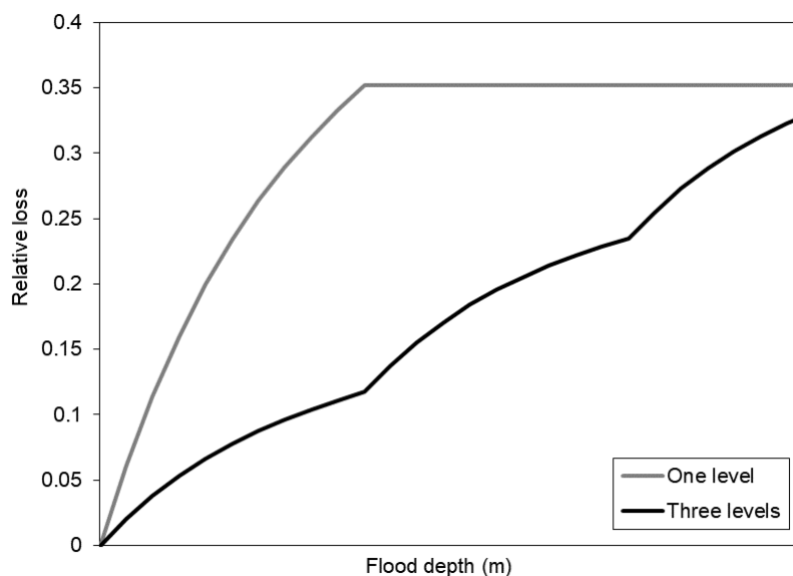


**Figure 4. Example of physical vulnerability function for tsunami (expected value)**

### Loss assessment and consideration of simultaneous perils

The assessment of damage and loss inflicted by simultaneous perils still represents a challenge when dealing with catastrophe risk models. This occurs mainly because of the lack of understanding between the effects of hazard intensities that affect, in a very short time frame, the same exposed asset. In the case of earthquakes and tsunamis, usually the ground motion affects first the exposed assets and later, within minutes, tsunami waves do the same. This means, in practical terms that the asset is first damaged by the ground motion and then, when the tsunami arrives, the vulnerability characteristics of that same element has changed (and increased).

To account for this issue and guaranteeing a complete compatibility of the assumptions within a fully probabilistic loss assessment framework, the methodology proposed by Ordaz (2015), on which simultaneous hazards are grouped into *temporalities*, provides a reasonable way of assessing damages and losses in multi-hazard environments. In a nutshell, all hazard that are assumed to occur in a simultaneous manner are grouped into the same *temporality*.

The loss for any event is therefore assessed by considering that the perils belonging to the same temporality occur in a simultaneous manner. Therefore, the loss for each of the exposed assets of relevance within the risk assessment process can be estimated with the following expression:

$$L_i = 1 - \prod_{j=1}^M (1 - L_{ij}) \quad (\text{Eq. 4})$$

where  $L_i$  is the loss associated to the  $i^{\text{th}}$  event,  $L_{ij}$  is the loss associated to the  $i^{\text{th}}$  event because of the action of peril  $j$  and  $M$  is the number of simultaneous perils considered in the temporality where the  $i^{\text{th}}$  event belongs. In this case, the values of  $L_{ij}$  are random variables, therefore,  $L_i$  is also a random variable.

At this point it is worth highlighting that, although the perils of interest for the case studies presented herein are earthquakes and tsunamis, the approach of grouping simultaneous hazards into temporalities can be expanded, without any limitation, to others as for instance, hurricanes (with strong winds, storm surge and floods as simultaneous perils) as well as landslides detonated by either earthquakes or excess of rain. The versatility of this approach allows its use in peril-agnostic risk assessment frameworks, such as the one implemented in R-CAPRA, which are those where the same methodology can be followed for the estimation of future losses regardless the types of peril, using of course, similar approaches for the characterization and representation of the hazard and vulnerability inputs.

## Case studies

### Acapulco, Mexico

#### Earthquake and Tsunamigenic Hazard

Acapulco is located at the coast of the Pacific Ocean, in the Guerrero state within the limits of the Cocos and North American tectonic plates, which is part of the Mesoamerican Trench characterized by being a high-seismicity zone. Historic evidence exists about damages due to simultaneous hazards and some of these data provide information about historical tsunamis, of local origin, which has affected Acapulco's seashores with ground motion and the entry of the ocean.

**Table 1. Wave heights for tsunamis of local origin in Acapulco prior to 1949**

<b>Date (DD/MM/YYYY)</b>	<b>Magnitude</b>	<b>Latitude</b>	<b>Longitude</b>	<b>Heights of run up [m]</b>	<b>Description</b>
28-03-1787	8.4 - 8.6	--	--	3 a 8	Magnitude between 8.4 and 8.6 seems credible. There are different data for waves heights reached, between 3 and 8 m in Acapulco. Literature refers to Acapulco village, what is a fraction of what the bay is today, so that 4 m is taken as height reached in the village for that time and it is believed that could be higher in other parts of the bay.
4-05-1820	7.6 - 8.0	17 .2	-99.6	4.0	It is mentioned that it is feasible that it was a large earthquake inland of magnitude 8 or two almost simultaneous since epicenter was inland.
11-03-1834	7.9	--	--	N/D	The sea retreated 10 m and recover its level gradually it is said that the earthquake occurred on March 11 and March 14, however explains that there was a succession of several earthquakes that generated fluctuations in the sea since March 11 and up to three days after.
7-04-1845	7.9	16 .6	-99.2	N/D	It is suggested that the tide penetrated approximately 40 m, the sea withdrew 35 m, there are documents of this tsunami in Michoacán, Guerrero, Oaxaca and Jalisco.
14-04-1907	7.6	16 .7	-99.2	1.85 a 2	The sea rose 1.85 m and go 150 meters land in these measures must be referred to the port of Acapulco. The quake occurred around 11:30 p.m. and the tsunami half an hour later.

Date (DD/MM/YYYY)	Magnitude	Latitude	Longitude	Heights of run up [m]	Description
30-07-1909	7.2 - 7.4	16 .8	-99.9	N/D	The amplitude of wave was 10 m, given the dimensions of the earthquake and the fact that much of Acapulco was destroyed by the earthquake, not by the tsunami, a wave height of 10 m is considered wrong and will be considered for this work which entered 10 m horizontally.

**Table 2. Wave heights for tsunamis of local origin in Acapulco after 1949**

Date	Magnitude	Latitude	Longitude	Heights of run up [m]	Description
28-jul-1957	7.8	17.11	-99.1	2.6	The earthquake of The Angel, the waves were presented with 20-minute period and oscillations lasted 20 hours.
11-may-1962	7.2	17.25	-99.58	0.75 a 0.81	The descent was 0.54 m; the wave came at 9 minutes from the epicenter 100 km from Acapulco.
19-may-1962	7.1	17.2	-99.57	0.3	The sea fell 0.27 m (run-down), but it did not come up more, only be matched again.
30-ene-1973	7.5	18.4	-103.2	0.4	The period was 28 minutes; and the arrival of the tsunami time: 45 minutes.
14-mar-1979	7.4 a 7.6	17.75	-101.263	1.31	Time between crests 30 min, the text is ambiguous; it says "maximum run-down 1.31 m".
19-sept-1985	8.1	18.419	-102.458	1.15	The tsunami came in 23 minutes.
21-sept-1985	7.6	17.828	-101.681	1.2	Propagation time was 19 minutes
20-mar-2012	7.4	16.662	-98.1870	0.2	In this case personal reference of the existence of tsunami was obtained by the earthquake of Ometepec.

Given the damage history, this is a good example for a probabilistic analysis of simultaneous events.

### **Relevance of this analysis**

Acapulco is one of the most visited locations by domestic tourists given its proximity to Mexico City and the diversity of leisure activities offered there, Figure 5 shows some photographs of Acapulco nowadays, bearing in mind that hotels in the peninsula's beaches were first developed around 1940 in the downtown area (Valenzuela and Coll-Hurtado, 2009), as well as at Acapulco Dorado zone, which was built after the 1960's. Finally, the urbanization of the Bay of Santa Lucia was completed in the 1970s.



**Figure 5. Aerial pictures of Acapulco nowadays. Bay of Santa Lucia (left) and Beach Diamante (right)**

### **Exposed assets and vulnerability**

A hazard-prone level classification of the schools has been made and it is represented by a shapefile created with the database of public schools provided by the SEP (Ministry of Education), through INIFED (Educational Infrastructure, in Spanish) and CAPFCE (School Construction Federal Program Administration Committee, in Spanish), with an asset-by-asset resolution level. For each school, its location, economic value (standard replacement cost, defined common costs per square meter and the total constructed area of each school), number of stories, structural type, and occupancy levels in terms of the number of students and staff were defined.

### **Hazard maps, risk and results**

Below, some hazard maps are presented for the city of Acapulco, which were obtained with the information from the \*.AME files<sup>2</sup> employed by R-CAPRA for this analysis. Figure 6 shows the earthquake hazard map corresponding to PGA and 100-year return period.

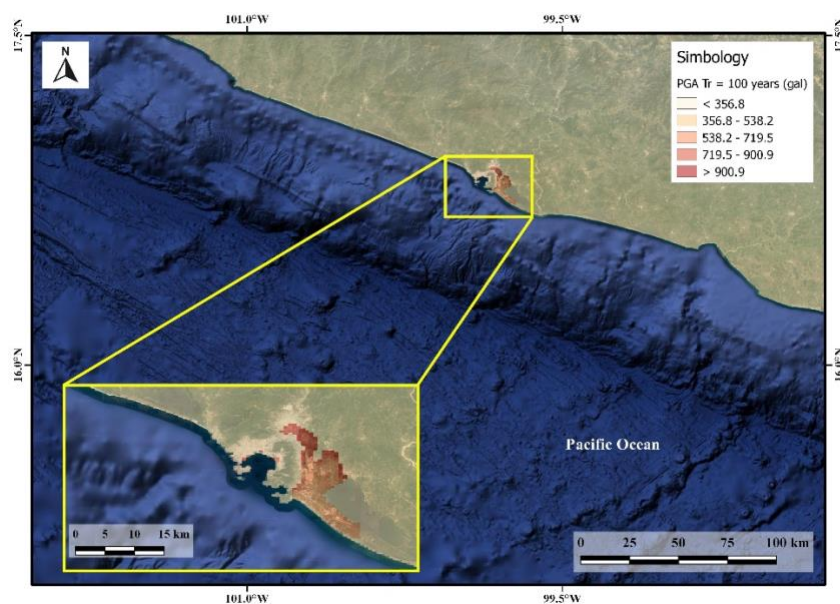


**Figure 6. Seismic hazard map for Acapulco. PGA ( $\text{cm/s}^2$ ) for 100-year return period**

In addition to the calculation of the hazard in firm soil (rock), information on the characteristics of the soil was used, obtained through environmental vibration measurements made on site and records of strong movement stations installed in Acapulco, available in the Mexican Base of Strong Earthquakes, to determine a map of soil iso-periods and spectral ratios.

For the amplification functions of each point we looked for functional relationships between each of the parameters of cross-sections available, in such a way that, elsewhere in the city, where there are no records, it was possible to estimate the transfer function of soil with the information of its period and with the help of a one-dimensional model. Figure 7 shows a map of key soil periods for the city of Acapulco. This information was adapted to R-CAPRA formats to be considered in the risk estimation.

<sup>2</sup> The format used in R-CAPRA for the event-based hazard representation

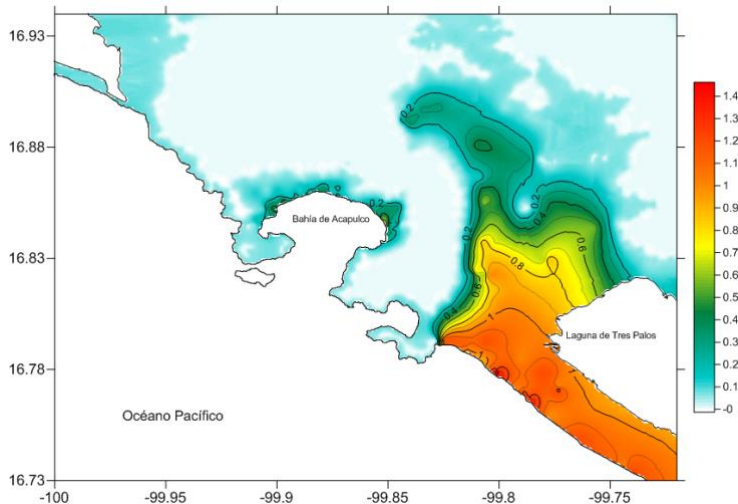


**Figure 7. Dominant soil periods for the urban area of Acapulco**

The most complete topography information available on the website of NASA's project ASTER Global with resolution of 1 "(approximately 30m) was used for the estimation of tsunami hazard, since this is the information with higher resolution available for the region. However, possible errors were found in some points, so data from other sources was integrated, in the case of Acapulco was used information generated by Mexico´s National Institute of Statistics and Geography (INEGI): a ground resolution LIDAR to every 5 meters and data from the CEM 3.0 @ 15 meters. Map in Figure 8 shows the inundation depth for the critical event of this database.

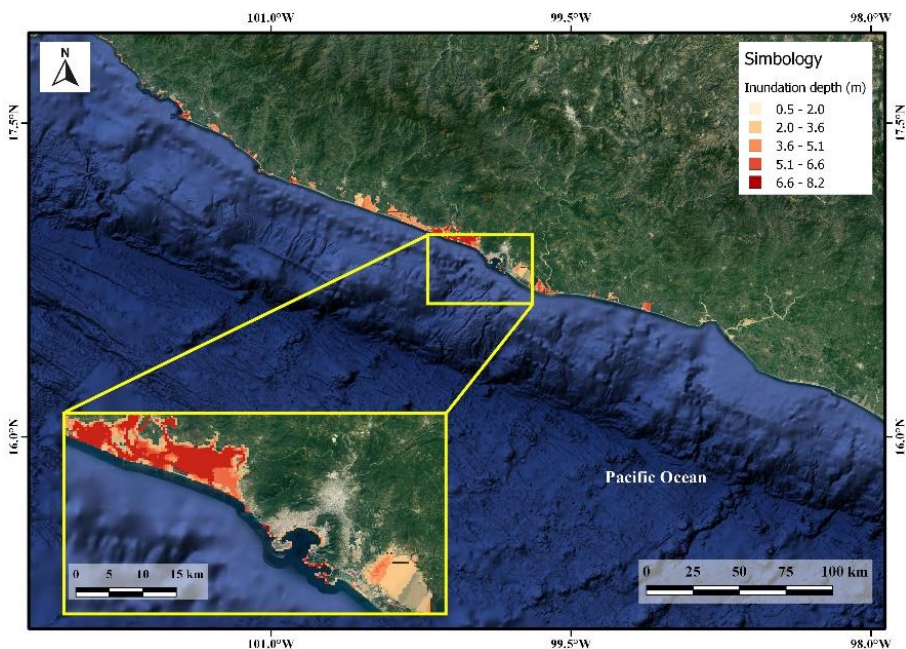


**Figure 8. Flooded zones for the critical event at Acapulco**

Results of the assessments are shown below, map in Figure 9 shows how higher relative losses for both hazards are closest to the coast, apparently dominated by tsunami hazard, although naturally the hazard of earthquake mastering the estimation of losses.

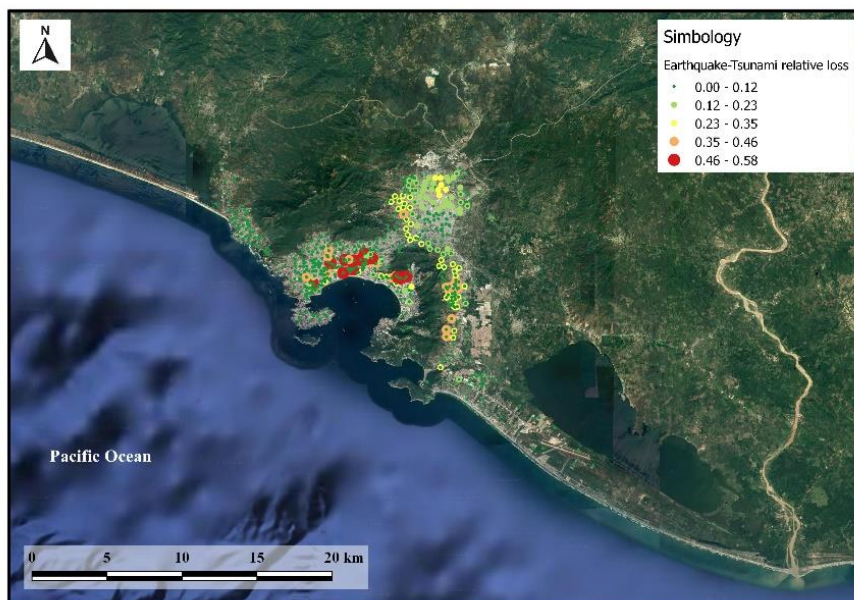


**Figure 9. Relative losses (considering simultaneous perils) for the critical scenario in Acapulco**

## **Callao, Peru**

### **Earthquake and Tsunamigenic Hazard**

El Callao is located on the central coast of Peru in the Department of Lima, tectonically at the interaction of the Nazca and South America plates, which have generated the largest seismic event registered. Like Acapulco, Callao has in its history several records of damage caused by both hazards, earthquake and tsunami, Table 3 show some examples.

**Table 3. Heights of waves recorded by tsunami of local origin in El Callao**

Date	Magnitude	Latitude	Longitude	Wave height [m]	Observations
10/07/1586	8.6	-12.1	-77	4	Tsunami off the coast of Lima, the sea level rose 4 m, the waves flooded part of the village of Callao, reaching the St. Domingo monastery (about 250 m).
20/10/1687	8.2	-13.2	-76.5	N/D	2 earthquakes occurred in Lima, the tsunami was triggered by the second earthquake.
29/10/1746	8.0-8.6	-12	-77.2	10	Callao disappears under the sea. The sea retreated but didn't return to its original limit which means that the whole area sank after the earthquake.
1/12/1806	N/D	-12	-78	6	The entire city shuddered for about a minute. Seaquake in Callao, waves of 6 m height ran aground an anchor of 1.5 ton on the Port Captain's house.
24/05/1940	8.0	-11.2	-77.8	2	Destruction of many buildings in Lima, Callao, Chancay and Lurín. A small tsunami was generated with mild floods in Ancón and Callao.
03/10/1974	7.8	-12.3	-77.5	1.8	Tsunami triggered by an earthquake off the coast of Callao, several factories were flooded in the Chimú and Tortugas bays north of Lima.

### Relevance of this analysis

The industrial port of Callao is one of the busiest in Peru with a large traffic and storage capacity. It is also one of the most important ports in the South Pacific region of Latin America. On the left of Figure 10 it is shown an aerial view of the port, which depicts the high density of population in this part of the metropoli of Lima and Callao. On the right, a map created by Peru's Navy shows inundation caused by tsunami for two proposed seismic events in Callao, the area encompassing the tip is for an event of  $M_w=8.5$  and area that extends beyond this area is for an event of  $M_w=9.0$ .



**Figure 10. Left: Aerial picture of the Callao Port (Source: Asociación Peruana de Agentes Marítimos).**

**Right: Flood hazard map of La Punta**

**Exposed assets and vulnerability**

For this study, the exposure database was obtained from proprietary data previously gathered by ERN, again with an asset-by-asset exposure database, where the characterization process makes use of different sources, such as existing databases, asset inventory, land and property value information, maps and plans of land use and territorial planning.

**Hazard maps, risk and results**

As for Acapulco, some hazard maps for Lima and Callao are presented which were obtained from AME files employed by R-CAPRA. Figure 11 shows the hazard map for earthquake corresponding to PGA and 100-years return period.

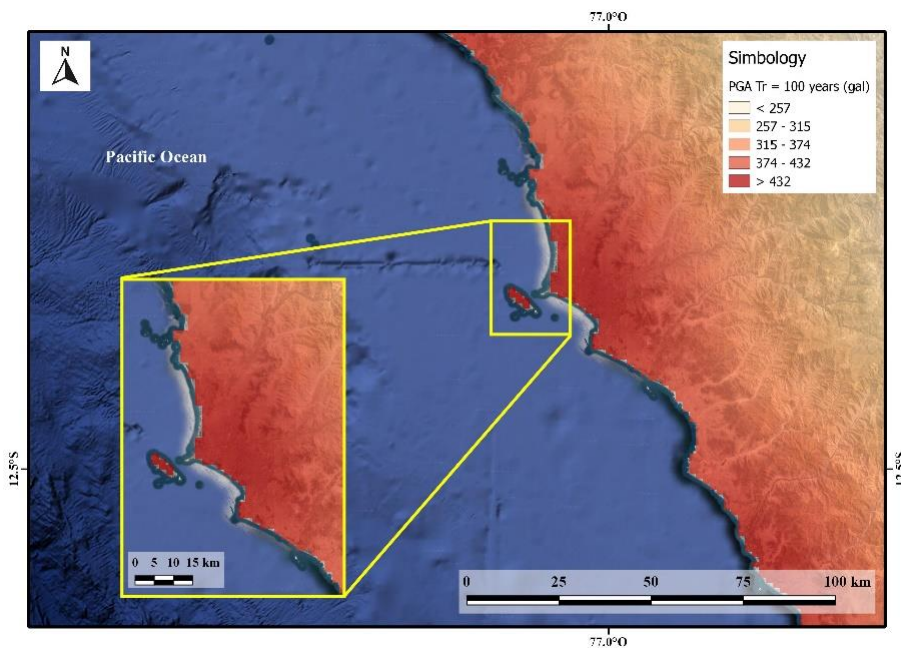


**Figure 11. Seismic hazard map for Lima and Callao. PGA ( $\text{cm/s}^2$ ) for 100-year return period**

For tsunami hazard was used the same NASA's topography, corrected with digitized information of the 2235 nautical chart of the Peru Navy. Given the importance of the port and the history of tsunamis in La Punta, Figure 12 show the results of relative loss for Tsunami in the considered exposure, verifying that the zone of greatest risk facing this hazard is the Callao region.

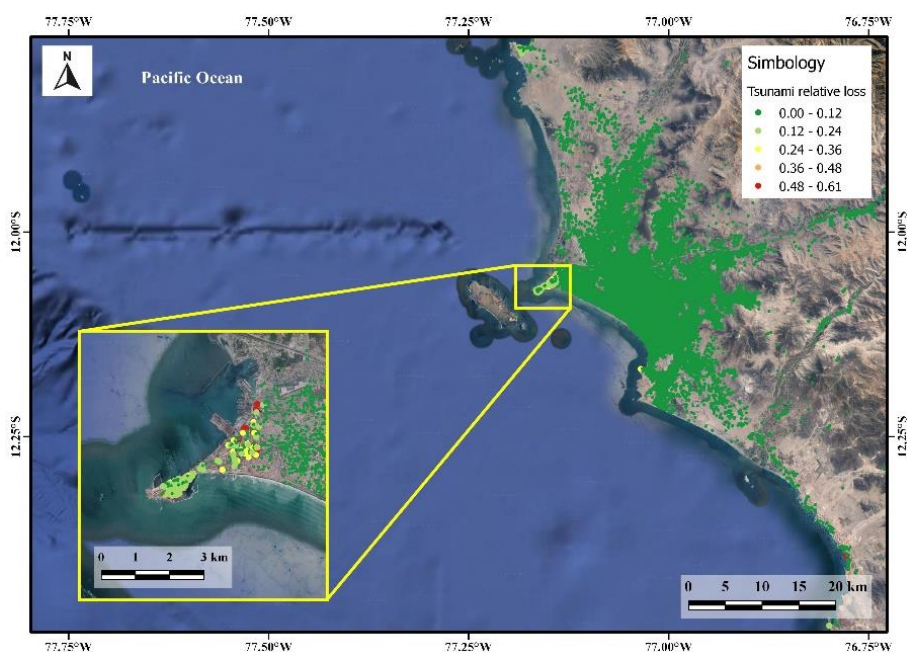


**Figure 12. Relative losses for tsunami considering the critical scenario**

Since for the full exposure of Lima and Callao earthquake hazard dominates completely the losses, an assessment was performed considering only the exposure which is affected by tsunami in order to show comparisons between the exceedance rates of losses for earthquake and tsunami. Figure 13 shows the exceedance rates of independent and simultaneous hazards for this exposure, it shows also that the sum of losses of independent hazards is lower than the corresponding to simultaneous ones.

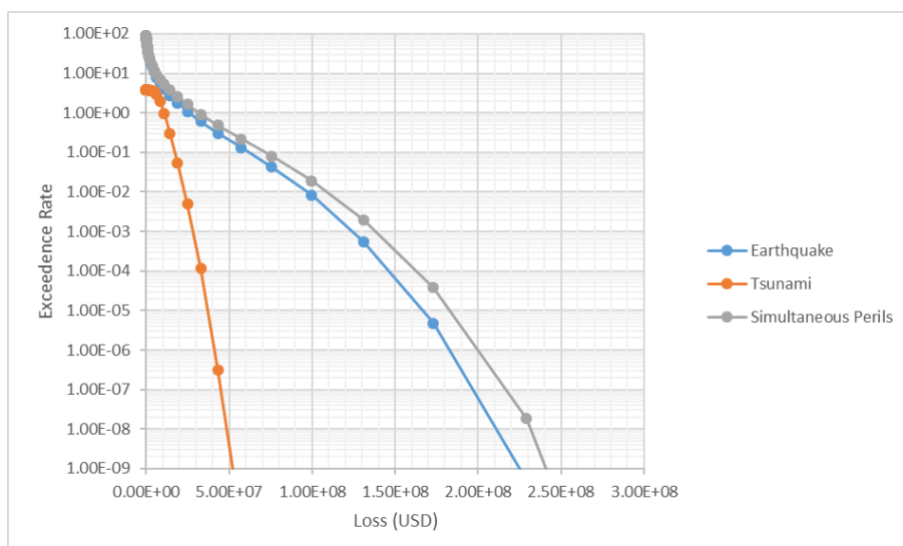


**Figure 13. Exceedance rates of losses for independent and simultaneous hazards**

## Results discussion and future research

To date, UNISDR's Global Risk Model (GRM) includes hazard, vulnerability and risk data for different perils such as earthquakes, tsunamis, riverine floods, cyclonic wind, storm surge and volcanic ash fall (the latter, only for some countries in the Pacific Region). Anyhow, and as already mentioned before, the quantification of the risk associated to these perils has been performed in a separate manner, leaving aside the relationships and interactions between them. This aspect can have consequences not only in the limitations of obtaining some risk metrics that fully account for the multi-hazard characteristics of the area under study, such as the loss exceedance curve and the probable maximum losses, but also variations in the average annual losses obtained in an individual manner and directly aggregated afterwards.

Given that the same probabilistic risk assessment framework and tools were used in the GRM (i.e., the former versions of R-CAPRA), the hazard representation using an event-based approach is already available for each of the perils, together with an exposure database, with global coverage that provides disaster risk information to more than 215 countries.

The global exposure database (GED) has been developed at two different resolution levels, 1x1km for the coastal areas only and 5x5km for inland locations. Given that tsunamis (as well as storm surge) has coastal affections, its risk assessment made use of the detailed one, whereas for seismic (as well as riverine flood and cyclonic wind) risk, the coarse-grained one was used.

For the case of earthquake and tsunami risk, what is missing can be split in two different components; 1) hazard analysis and 2) exposure databases. For the first component, and given that the hazard analyses were conducted in a separate way and using different approaches, at least for the subduction zone areas a comprehensive PSHA needs to be developed to generate not only the synthetic earthquakes but to identify which of them can trigger tsunamis and with them, obtain subsequently the associated synthetic tsunamis. This one-to-one association is needed in the methodological framework that has been presented in this paper and also, if performed, can increase considerably the resolution level of the PSHA, currently made at 30x30km, approximately. Being a peril-agnostic methodology, the interaction between other hazards included in the GRM can be accounted for, as for instance, grouping into the same temporality the cyclonic wind and storm surge perils.

For the second component, a unique exposure database needs to be used in the risk assessment process when accounting for simultaneous perils. In that sense, it would be desirable that a 1x1km global exposure database for inland and coastal locations can be developed. When developing the first version of the GRM, the 5x5km resolution for the exposure database was chosen mostly because of computation restrictions and not because there were not enough data to develop the exposure database with a higher resolution level. Not only today's computers provide higher performance levels but also, the R-CAPRA system has incorporated a parallelized process that speeds-up the computation times up to ten times, if compared with the original version, meaning that there are not technological barriers for the development and use of a higher resolution level.

If future versions of the GRM include the interaction and interdependencies of the different hazards using the methodological approach presented herein, the multi-hazard component will be available for all the risk metrics and not only to the AAL, which, although useful by summarizing in a single number the contribution of small, moderate and large events for the domain under study, is not sufficient for the design and implementation of a comprehensive disaster risk management strategy that should account for different timeframes (e.g., by making use of PMLs associated to different return periods) or by designing risk transfer mechanisms that need, among other inputs, annual exceedance probabilities for different loss values.

Although seismic and tsunami hazards are closely related, the methodological frameworks for their hazard and risk assessment are very different. Opposite to PSHA, the probabilistic approach for the tsunami hazard analysis is relatively new and therefore, more complicated tasks such as the vulnerability characterization and of course the risk assessment, lack of a formal framework widely accepted by the scientific community. As a response to that problem, the tsunamigenic scientific community has started the Global Tsunami Model (GTM), of which ERN

is part of, from which it is expected that not only guidelines but a common framework for the probabilistic tsunami risk assessment is made available. Among the approaches that are to be explored, agnostic and fully probabilistic ones such as the presented herein and implemented in R-CAPRA are included.

## References

- Arcos, M.E., LeVeque, R.J. (2013). Validation velocities in the Geoclaw tsunami model using observation near Hawaii from the 2011 Tohoku tsunami. *J. Geophys. Res.* 1-15.
- Berger, M.J., George, D.L., LeVeque, R.J., Mandli, K.T. (2011). The GeoClaw software for depth-averaged flows with adaptive refinement. *Adv. Water Res.* 34, 1195-1206.
- Cornell C.A. (1968). Engineering seismic risk analysis. *Bulletin of the Seismological Society of America.* 58(5):1583-1606.
- ERN – Evaluación de Riesgos Naturales (2018). R-CAPRA. Program for probabilistic and multi-hazard risk assessment. Mexico City, Mexico.
- Esteva L. (1967). Criterios para la construcción de espectros de diseño sísmico. In *Proceedings, 3rd Pan-American Symposium of Structures*, Caracas, Venezuela.
- González, F., LeVeque, R.J., Varkovitzky, J., Chamberlain, P., Hirai, B., George, D.L. (2011). GeoClaw Results for the NTHMP Tsunami Benchmark Problems. <http://depts.washington.edu/clawpack/links/nthmp-benchmarks/geoclaw-results.pdf>.
- Hanks, T.C., Kanamori, H. (1979). A moment magnitude scale. *J. Geophys. Res.* 84 (5), 2348-2350
- Jaimes M.A., Reinoso E., Ordaz M., Huerta B., Silva R., Mendoza E. and Rodríguez J.C. (2016). *Ocean & Coastal Management.* 119:68-75.
- LeVeque, R.J. (2002). *Finite Volume Methods for Hyperbolic Problems.* Cambridge University Press.
- LeVeque, R.J., George, D.L. (2007). High-resolution finite volume methods for the shallow water equations with bathymetry and dry states. In: Liu, C.S.P.L.-F., Yeh, H. (Eds.), *Advanced Numerical Models for Simulating Tsunami Waves and Runup*, 10, pp. 43-73. <http://www.amath.washington.edu/rjl/pubs/catalina04/>.
- LeVeque, R.J., George, D.L., Berger, M.J. (2011). Tsunami modeling with adaptively refined finite volume methods. *Acta Numer.* 211-289.
- Okal, E.A., Synolakis, C.E. (2004). Source discriminants for near-field tsunamis. *Geophys. J. Int.* 158, 899-912.
- Ordaz M. (2015). A simple probabilistic model to combine losses arising from the simultaneous occurrence of several hazards. *Natural Hazards.* 76(1):389-396.
- Singh, S.K., Pérez-Campos, X., Iglesias, A., Melgar, D. (2012). A method for rapid estimation of moment magnitude for early tsunami warning based on coastal GPS networks. *Seismol. Res. Lett.* 83 (2), 516-530.

UNISDR – United Nations International Strategy for Disaster Risk Reduction. (2013). Global Assessment Report on Disaster Risk Reduction 2013. Geneva, Switzerland.

UNISDR – United Nations International Strategy for Disaster Risk Reduction. (2015a). Global Assessment Report on Disaster Risk Reduction 2015. Geneva, Switzerland.

UNISDR – United Nations International Strategy for Disaster Risk Reduction. (2015b). Sendai Framework for Disaster Risk Reduction 2015-2030.

UNISDR – United Nations International Strategy for Disaster Risk Reduction. (2017). GAR Atlas. Geneva, Switzerland.

Valenzuela Valdivieso, E. y A. Coll-Hurtado (2009), “La construcción y evolución del espacio turístico de Acapulco (México)”, en Anales de Geografía, vol. 30, núm. 1, pp. 163-190.